RESEARCH FRONT

CSIRO PUBLISHING

Journal of Southern Hemisphere Earth Systems Science, 2019, **69**, 16–28
https://doi.org/10.1071/ES19021

The Antarctic ozone hole during 2015 and 2016

Matthew B. Tully[A], *Andrew R. Klekociuk*[B,C,J], *Paul B. Krummel*[D], *H. Peter Gies*[E], *Simon P. Alexander*[B,C], *Paul J. Fraser*[A], *Stuart I. Henderson*[E], *Robyn Schofield*[F,G], *Jonathon D. Shanklin*[H] and *Kane A. Stone*[I]

[A]Bureau of Meteorology, Melbourne, Vic., Australia.
[B]Antarctica and the Global System, Australian Antarctic Division, 203 Channel Highway, Kingston, Tas. 7050, Australia.
[C]Antarctic Climate and Ecosystems Cooperative Research Centre, Hobart, Tas., Australia.
[D]Climate Science Centre, CSIRO Oceans and Atmosphere, Aspendale, Vic., Australia.
[E]Australian Radiation Protection and Nuclear Safety Agency, Melbourne, Vic., Australia.
[F]School of Earth Sciences, University of Melbourne, Melbourne, Vic., Australia.
[G]ARC Centre of Excellence for Climate System Science, University of New South Wales, Sydney, NSW, Australia.
[H]British Antarctic Survey, Cambridge, United Kingdom.
[I]Massachusetts Institute of Technology, Cambridge, MA, United States of America.
[J]Corresponding author. Email: Andrew.Klekociuk@aad.gov.au

Abstract. We reviewed the 2015 and 2016 Antarctic ozone holes, making use of a variety of ground-based and space-based measurements of ozone and ultraviolet radiation, supplemented by meteorological reanalyses. The ozone hole of 2015 was one of the most severe on record with respect to maximum area and integrated deficit and was notably long-lasting, with many values above previous extremes in October, November and December. In contrast, all assessed metrics for the 2016 ozone hole were at or below their median values for the 37 ozone holes since 1979 for which adequate satellite observations exist. The 2015 ozone hole was influenced both by very cold conditions and enhanced ozone depletion caused by stratospheric aerosol resulting from the April 2015 volcanic eruption of Calbuco (Chile).

Received 22 January 2018, accepted 13 May 2019, published online 11 June 2020

1 Introduction

The Antarctic ozone hole has continued to appear each spring since its first detected appearance in 1979. Although the underlying mechanism of the ozone hole is now considered well understood, recent further work (Douglass *et al.* 2014; Solomon *et al.* 2014; Kirner *et al.* 2015; Solomon *et al.* 2015; Zhu *et al.* 2017) has continued to developed the detailed understanding of the formation of polar stratospheric clouds (PSCs), and the relative contribution of the different types of PSCs and chemical processes which lead to chlorine activation, and then prevent chlorine deactivation, during spring. The variability of reactive forms of chlorine inside the vortex from year to year has been identified (Strahan *et al.* 2014), including that due to quasi-biennial oscillation (QBO)-influenced transport (Strahan *et al.* 2015). The significant amount of chemical ozone depletion caused by anthropogenic ozone-depleting substances prior to the year 1980 was studied by Langematz *et al.* (2016), whereas the impact on Antarctic ozone of the eruption of the Chilean volcano Calbuco in April 2015 has also been investigated (Ivy *et al.* 2017; Stone *et al.* 2017).

Solomon *et al.* (2016) used a combination of modelling and observations to claim that a significantly positive trend in September mean ozone of 2.5 ± 1.7 DU/year could be attributed to declining halogen levels, most markedly in the height range between 100 and 50 hPa.

In this paper, we provide a description of the level of Antarctic ozone depletion in 2015 and 2016 and the relationship with prevailing meteorological conditions using a range of Australian data and analyses including measurements and analyses by the Commonwealth Scientific and Industrial Research Organisation (CSIRO) Oceans and Atmosphere unit, ozone measurements made by the Australian Antarctic Division (AAD) and the Bureau of Meteorology (BoM), and Antarctic ultra-violet measurements from the Australian Radiation Protection and Nuclear Safety Agency (ARPANSA) biometer network. Other data from satellite missions and ground-based instruments are also presented. This work complements the analyses of previous Antarctic ozone holes reported by Tully *et al.* (2008, 2011) and Klekociuk *et al.* (2011, 2014*a*, 2014*b*, 2015), Krummel *et al.* (2019) and other analyses of Antarctic atmospheric conditions and ozone depletion during 2015 and 2016 provided by the CSIRO (Krummel *et al.* 2016, 2017; http://www.environment.gov.au/protection/ozone/publications/antarctic-ozone-hole-summary-reports, accessed

21 April 2020), the World Meteorological Organisation (WMO) Antarctic Ozone Bulletins (http://www.wmo.int/pages/prog/arep/gaw/ozone/index.html, accessed 21 April 2020), upper air summaries of the National Climate Data Center (NCDC; http://www.ncdc.noaa.gov/sotc/upper-air, accessed 21 April 2020) and by Weber *et al.* (2016, 2017; http://www.ncdc.noaa.gov/bams-state-of-the-climate, accessed 21 April 2020).

2 Total column ozone measurements

2.1 Ozone hole metric summary and rankings

As in previous reports in this series, we use total column ozone measurements from satellite instruments to obtain metrics of the Antarctic ozone hole for each year (see Klekociuk *et al.* (2015) for details). Here we use data processed with the version 8.5 TOMS algorithm from the Total Ozone Mapping Spectrometer (TOMS) series of satellite instruments, the Ozone Monitoring Instrument (OMI) on the Aura satellite and the Ozone Mapping Profiler Suite (OMPS) on the Suomi National Polar-orbiting Partnership satellite.

Table 1 contains the ranking for the 37 ozone holes adequately observed by satellite instruments since 1979 using eight metrics that provide different measures of the extent of ozone depletion in each year (see the notes accompanying the table for the definition of each metric). The first seven metrics in Table 1 measure various aspects of the maximum area and depth of the ozone hole. These metrics highlight the contrasting behaviours of the ozone holes of 2015 and 2016. The 2015 ozone hole was ranked between 3rd and 16th in terms of severity across these metrics, with the maximum 15-day averaged area of 27.6 Mkm^2 (central date 5 October 2015) equalling the value set in 2006 (central date 22 September 2006) which has only been exceeded by the ozone hole of 2000 (28.7 Mkm^2, central date 6 September 2000). Rankings for the metrics relating to minimum ozone values were lower (12th–16th) than those for area (3rd–4th) or deficit (5th–7th). In contrast, the ozone hole of 2016 was ranked between 17th and 21st for all metrics and exhibited quantitative similarity with ozone holes of the late 1980s-early 1990s and some recent years, particularly 2010 and 2014.

Figure 1 shows the time-series of the ozone hole area, minimum polar total column ozone and total ozone deficit within the ozone hole over the latter half of each year from 2009 to 2016. Notable features of the metrics shown in Fig. 1 for 2015 are the relatively delayed development of the ozone hole (which started showing significant growth in late August, 1–2 weeks later than most of the years since 2011) and late peak (which occurred in early October, ~2 weeks later than the long-term averages). Furthermore, the metrics during the declining phase were at or near record levels throughout the period from October to mid-December and exhibited relatively little in the way of week-to-week fluctuations that normally occur in this period due to warming of the polar vortex. The date of breakdown (column 8 in Table 1) for 2015 was one of the latest on record.

In the case of 2016, the metrics shown in Fig. 1 were more typical of the long-term mean and generally intermediate between the behaviours seen in 2013 and 2014. Notably, there was a rapid decline in the area metric (Fig. 1*a*) through most of October which gave way to a short hiatus (lasting ~2 weeks up to early November) during which there was slight growth. Subsequently, there was again rapid decline in the size of the hole, and the final breakdown occurred on 20 November, which was similar to the behaviour seen in 2012 and 2013, and generally earlier than the long-term average.

Details of the meteorological conditions in 2015 and 2016 influencing these results are presented in Appendix 1.

Figure 2 shows the estimated total annual ozone deficit associated with the Antarctic ozone hole. This metric shows large year-to-year variability which largely reflects meteorological factors, with a disturbed polar vortex or relatively warm stratospheric temperatures producing a relatively low deficit, such as for 2002, 2004 and 2012, and cold stratospheric temperatures or a relatively long-lived polar vortex creating a large deficit, such as for 1998–2001 and 2006. The annual deficit in 2015 of 2197 Mt was the 5th largest observed.

Also shown in Fig. 2 is the estimated level of Antarctic equivalent effective stratospheric chlorine (EESC; orange line) from Fraser *et al.* (2014), which is a measure of the potential for ozone depletion in the lower stratosphere.

A longer term data record is available from ground-based Dobson spectrophotometer measurements at the British Antarctic Survey's Halley station (75.6°S and 26.2°W) in Antarctica (BAS 2015). Figure 3 shows mean October total column ozone from 1957 to 2016, again together with Antarctic EESC (Fraser *et al.* 2014; Klekociuk *et al.* 2015). The Halley average value for October 2015 shown in Fig. 3 of 139 DU was similar to that measured in years of notably severe ozone loss (Klekociuk *et al.* 2015); 2000 (137 DU), 2001 (138 DU), 2006 (137 DU) and 2011 (140 DU). The mean October total column ozone value at Halley over 2011–16 (157 ± 18 DU) is higher than that over 1996–2001 (141 ± 4 DU), but the difference is not statistically significant at the 95% confidence threshold (1 standard error in mean values are quoted). Over the years 1996–2016, ignoring the dynamically disturbed years of 2002 and 2004 (Klekociuk *et al.* 2015), the linear trend is 1.0 ± 1.0 (2σ) DU/year. As studied by Langematz *et al.* (2016), it is apparent from Fig. 2 that Antarctic ozone depletion was quite significant in the decade from 1970 to 1980 notwithstanding the general use of 1980 as the baseline year for ozone depletion and subsequent recovery.

3 Vertically resolved ozone measurements

3.1 Davis ozonesondes

Figure 4 shows the 12–20 km partial column ozone amount for all available ozonesonde measurements from Australia's Davis research station in Antarctica (68.6°S and 78.0°E). Ozonesonde flights during 2015 were restricted to approximately monthly intervals for most of the year following logistical difficulties in supplying consumables to Davis.

The rate of ozone decreases between days 240 and 270 (approximately the month of September) has been quite consistent over the 2003–16 period; however, the minimum value eventually reached, as well as the timing and rate of the following increase, varies significantly from year to year. During the months of October (day-of-year 274–304) and November (day-of-year 305–334), the location of Davis at times can lie outside the ozone hole depending on the size and shape of

Table 1. Ranked Antarctic ozone hole metrics obtained from TOMS/OMI/OMPS satellite data

TOMS data are used from 1979 to 2014, OMI data are used for 2005–15 and OMPS data are used for 2016. Data for 2015 and 2016 are highlighted in bold. *Note*: In previous papers in this series (Tully *et al.* 2008, 2011; Klekociuk *et al.* 2011, 2014*a*, 2014*b*, 2015), the Antarctic ozone hole metrics for the year 2005 were an average of both TOMS and OMI data, and hence the 2005 rankings in those papers will differ from those quoted below. Rank 1 is the lowest ozone minimum, greatest area, greatest ozone loss etc.; Rank 2 is the second lowest ozone minimum, etc. There was a gap in TOMS coverage during the growth of the 1994 ozone hole; metrics for some parameters for that year are, therefore, undetermined and are left blank. There were no relevant TOMS measurements in 1995. Metric definitions: (1) Maximum 15-day averaged area: the largest value (in each year) of the daily ozone hole area averaged using a 15-day sliding time interval. (2) Daily maximum area: the maximum daily value of the ozone hole area. (3) Minimum 15-day averaged total column ozone: the minimum of the 15-day averaged column ozone amount observed south of 35°S. (4) Daily minimum total column ozone: the minimum of the daily column ozone amount observed south of 35°S. This metric effectively measures the 'depth' of the ozone hole. (5) Daily minimum average total column ozone: the minimum of the daily column ozone amount averaged within the ozone hole. This metric effectively measures the 'average depth' of the ozone hole. (6) Maximum daily ozone deficit: the maximum value of the daily total ozone deficit within the ozone hole. This metric effectively measures the combined area and depth of the ozone hole. (7) Integrated ozone deficit: the integrated (total) daily ozone deficit for the entire ozone hole season. This metric effectively measures the overall severity of ozone depletion. (8) Breakdown date: The final date at which the daily maximum area (metric 2) falls below 0.5 million km^2. Note that the metrics use 220 DU as the threshold in total column ozone to define the location and occurrence of the ozone hole

Metric	(1) Maximum 15-day averaged area		(2) Daily maximum area		(3) Minimum 15-day averaged total column ozone		(4) Daily minimum total column ozone		(5) Daily minimum average total column ozone		(6) Daily maximum ozone deficit		(7) Integrated ozone deficit		(8) Breakdown date	
Rank	Year	10^6 km^2	Year	10^6 km^2	Year	DU	Year	DU	Year	DU	Year	Mt	Year	Mt	Year	Date (day)
1	2000	28.7	2000	29.8	2000	93.5	2006	85	2000	138.3	2006	45.1	2006	2560	1999	27-December (361)
2	2006	27.6	2006	29.6	2006	93.7	1998	86	2006	143.6	2000	44.9	1998	2420	2008	26-December (361)
3	**2015**	**27.6**	2003	28.4	1998	96.8	2000	89	1998	146.7	2003	43.4	2001	2298	2010	21-December (355)
4	2003	26.9	**2015**	**28.1**	2001	98.9	2001	91	2003	147.5	1998	41.1	1999	2250	**2015**	**20-December (354)**
5	1998	26.8	1998	27.9	1999	99.9	2003	91	2001	148.8	2008	39.4	**2015**	**2197**	2001	19-December (353)
6	2008	26.1	2005	27.2	2011	100.9	1991	94	1999	149.3	2001	38.5	1996	2176	2011	19-December (353)
7	2001	25.7	2008	26.9	2003	101.9	2011	95	2005	149.4	**2015**	**37.7**	2000	2164	2006	16-December (350)
8	2005	25.6	1996	26.8	2009	103.1	2009	96	2009	150.4	2011	37.5	2011	2124	1990	15-December (349)
9	2011	25.1	2001	26.4	1993	104.0	1999	97	1996	150.6	2005	37.1	2008	1983	2007	15-December (349)
10	1996	25.0	2011	25.9	1996	106.0	1997	99	2008	150.8	2009	35.7	2003	1894	1998	13-December (347)
11	1993	24.8	1993	25.8	**2015**	**107.1**	**2015**	**101**	2011	151.2	1999	35.3	2005	1871	2005	11-December (345)
12	1994	24.3	1999	25.7	1997	107.2	2008	102	1997	151.3	1997	34.5	1993	1833	1992	08-December (343)
13	2007	24.1	1994	25.2	2008	108.9	2004	102	2007	155.1	1996	33.9	2009	1806	1996	08-December (343)
14	2009	24.0	2007	25.2	2005	108.9	1996	103	1993	155.2	1992	33.5	2007	1772	1987	08-December (342)
15	1992	24.0	1997	25.1	1992	111.5	2005	103	1992	156.3	2007	32.9	1997	1759	2004	05-December (340)
16	1999	24.0	1992	24.9	2007	112.7	1993	104	**2015**	**156.9**	1993	32.6	1992	1529	2003	05-December (339)
17	1997	23.3	2009	24.5	1991	113.4	1992	105	**2016**	**159.7**	2014	30.7	1987	1366	1993	04-December (338)
18	2013	22.7	2013	24.0	1987	115.7	1989	108	2014	160.0	**2016**	**29.3**	2010	1353	1985	03-December (337)
19	2014	22.5	2014	23.9	2004	116.0	2007	108	1991	162.5	1991	26.6	2014	1252	1997	03-December (337)
20	**2016**	**21.6**	**2016**	**22.7**	**2016**	**117.5**	1987	109	1987	162.6	2010	26.2	**2016**	**1218**	1989	01-December (335)
21	2010	21.6	2004	22.7	1990	117.8	**2016**	**111**	1990	164.4	1987	26.2	1990	1181	1984	28-November (333)
22	1987	21.4	1987	22.4	1989	120.4	1990	111	2010	164.5	2013	25.1	2013	1037	2009	29-November (333)
23	2004	21.1	1991	22.3	2014	124.3	2014	114	2013	164.7	1990	24.3	1991	998	1994	25-November (329)
24	1991	21.0	2010	22.3	2010	124.3	2013	116	1989	166.2	1989	23.6	2004	975	**2016**	**20-November (325)**

25	1989	20.7	2002	21.8	2013	127.8	2010	119	2004	166.7	2002	23.2	1989	917	2000	19-November (324)
26	1990	19.5	1989	21.6	1985	131.8	2012	124	2002	169.8	2004	22.8	2012	720	1991	18-November (322)
27	2012	19.3	2012	21.2	2012	131.9	1985	124	2012	170.2	2012	22.5	1985	630	2013	16-November (320)
28	2002	17.7	1990	21.0	2002	136.0	2002	131	1985	177.1	1985	14.5	2002	575	1986	14-November (318)
29	1985	16.6	1985	18.6	1986	150.3	1986	140	1986	184.7	1986	10.5	1986	346	1982	12-November (316)
30	1986	13.4	1984	14.4	1984	156.1	1984	144	1984	190.2	1984	9.2	1984	256	2012	07-November (312)
31	1984	13.0	1986	14.2	1983	160.3	1983	154	1983	192.3	1983	7.0	1988	198	1980	06-November (311)
32	1988	11.3	1988	13.5	1988	169.4	1988	162	1988	195.0	1988	6.0	1983	184	2002	06-November (310)
33	1983	10.1	1983	12.1	1982	183.3	1982	170	1982	199.7	1982	3.7	1982	73	1983	05-November (309)
34	1982	7.5	1982	10.6	1980	200.0	1980	192	1980	210.0	1980	0.6	1980	13	1981	31-October (304)
35	1980	2.0	1980	3.2	1981	204.0	1979	194	1979	210.2	1981	0.6	1981	4	1988	26-October (300)
36	1981	1.3	1981	2.9	1979	214.7	1981	195	1981	210.2	1979	0.3	1979	1	1979	19-September (262)
37	1979	0.2	1979	1.2	1994		1994	-	1994		1994		1994		1994	

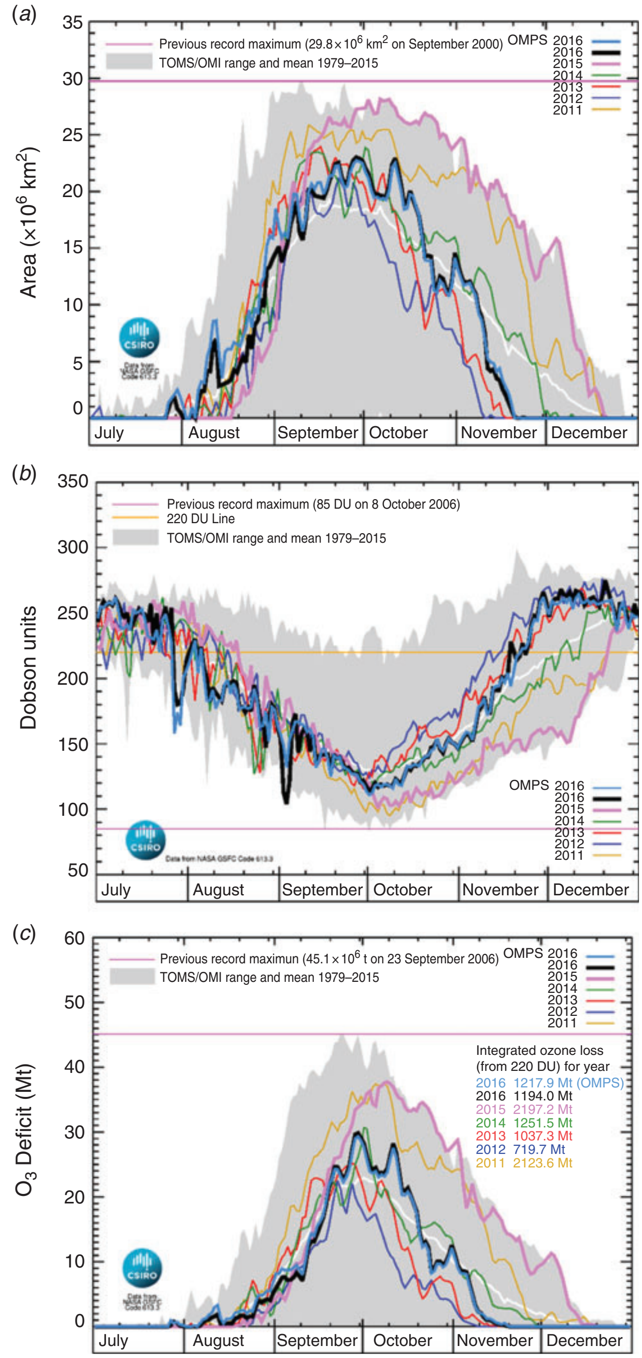

Fig. 1. Estimated daily (*a*) ozone hole area, (*b*) ozone hole depth and (*c*) ozone mass deficit based on OMI satellite data for 2011–16 and OMPS satellite data for 2016. The shaded region and white line show the range and mean respectively over 1979–2015.

the hole, leading to the observed spikes in 2015 and more particularly, 2016.

Further detail of the course of depletion in 2015 and 2016 compared to previous years can be seen by breaking down the partial column into the following three narrower height ranges, 12–15, 15–18 and 18–21 km (Fig. 5*a*–*c*).

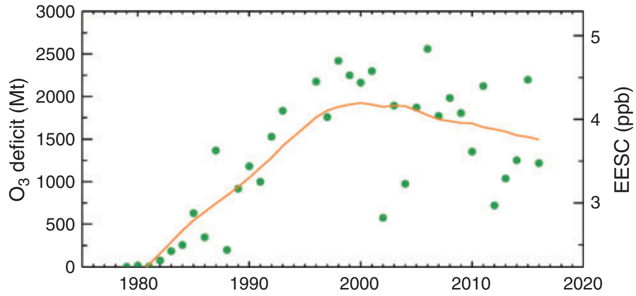

Fig. 2. Estimated total ozone deficit for each year in millions of tonnes (Mt), based on TOMS (1979–2004), OMI (2005–15) and OMPS (2016) satellite data. The orange line is obtained from a linear regression to EESC (expressed in parts per billion by volume) from Fraser *et al.* (2014) using a mean age of air of 5 years.

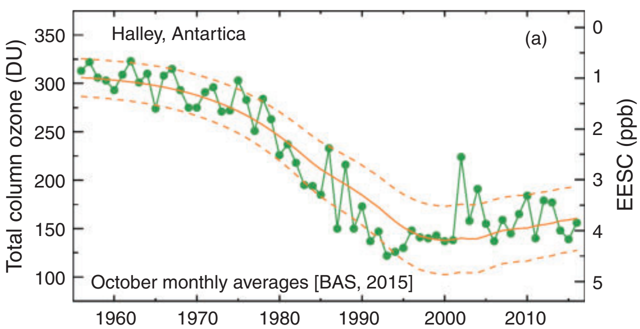

Fig. 3. October monthly mean total column ozone values for Halley station for 1957–2014 (green points and line; BAS 2015) and regression to EESC (orange line) from Fraser *et al.* (2014) using a mean age of air of 5 years. (Dashed orange lines show the 95% uncertainty limits of the regression.)

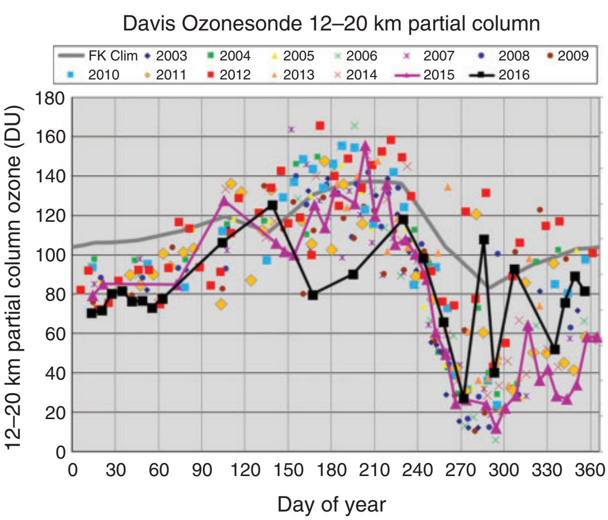

Fig. 4. Time-series of partial column ozone for the height interval 12–20 km obtained from ozonesonde measurements at Davis, Antarctica (68.6°S and 78.0°E). Shown are data for all years of measurement, with data for 2015 highlighted with filled magenta triangles and solid line and 2016 highlighted with black-filled squares and solid line. The grey line is a climatological mean from Fortuin and Kelder (1998) interpolated to the location of Davis. Note that at Davis, this height range is almost exclusively above the lapse rate tropopause and generally below the burst height of the ozonesonde balloons in winter.

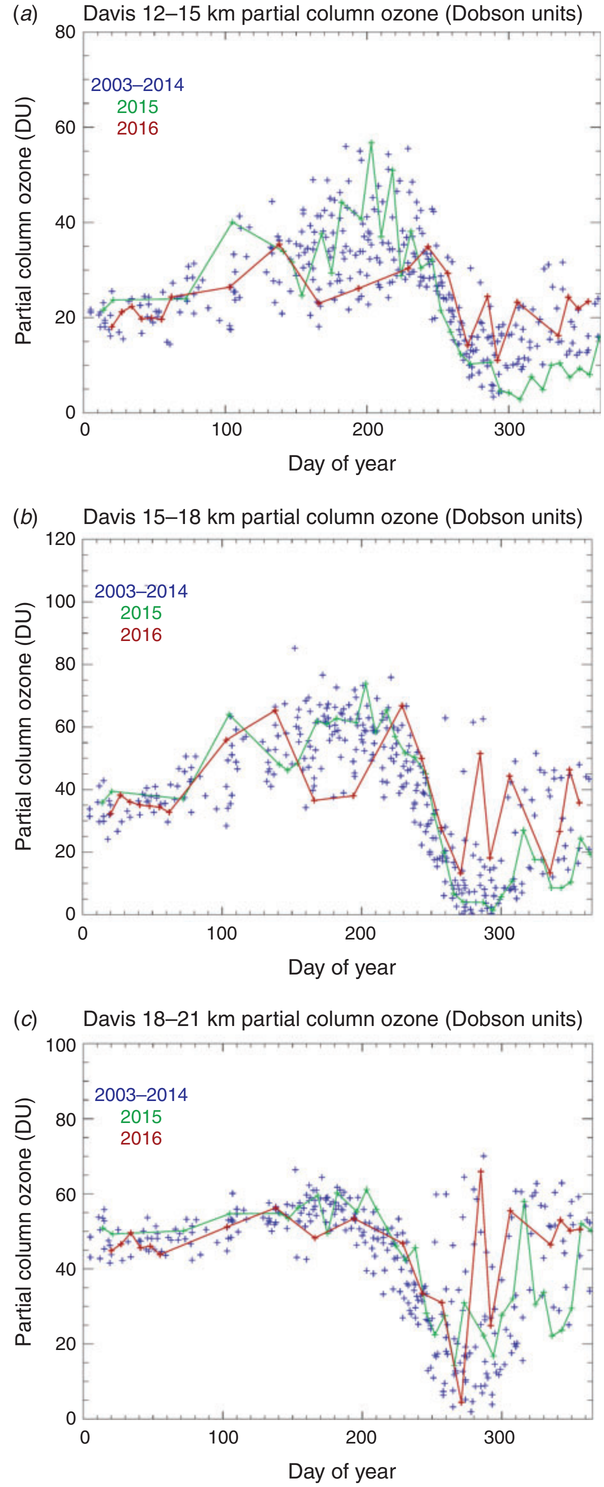

Fig. 5. Partial ozone columns measured by Davis ozonesondes between (*a*) 12 and 15 km, (*b*) 15 and 18 km (*c*) 18 and 21 km.

The 12–15 km partial column ozone was slightly below the long-term record during the period of decline in September in 2015 and slightly above in 2016; however, the more noteworthy feature was the series of very low values recorded in November and December 2015 after the minimum had been reached, well below those previously seen in the Davis record (2003 onwards). In contrast, in 2016 the 12–15 km partial column was never reduced to the very low ozone values observed in many previous years and recovered steadily.

The 15–18 km partial columns decayed during September somewhat later (10 days) than is typical for the Davis record in both 2015 and 2016, as noted earlier with respect to the area of the ozone hole. Values stayed very low for several weeks in October in 2015 and only slowly recovered. In 2016 this height range showed large variability as the position of Davis relative to the vortex shifted from week to week.

In contrast, the 18–21 km partial column did not display exceptionally low values in 2015, and in fact most other years since 2003 have recorded lower annual minima in this height range. In 2016, a single ozonesonde flight (27 September 2016) measured almost zero ozone (0.23 mPa) at 19.7 km (43 hPa); however, values were much higher after this date for the rest of the year.

The difference in behaviour within the respective partial columns is consistent with the finding of Stone *et al.* (2017) that the impact on ozone of volcanic aerosol transported polewards from Calbuco (Chile) was concentrated between 150 and 100 hPa (approximately corresponding to 12–15 km in altitude).

3.2 Aura microwave limb sounder stratospheric ozone profiles

Annual values of the vortex-average rate-of-change of ozone mixing ratio as a function of temperature, averaged over days 200–260 (19 July–17 September in nonleap years), for isentropic levels of potential temperature (θ) equal to 450 K (~18 km height) and $\theta = 850$ K (~31 km height), are shown in Fig. 6*a*, *b*, for years 2004–16. These figures essentially summarise characteristics during the period when the ozone hole is generally growing. The values are obtained from Aura microwave limb sounder (MLS) version 4.2 data as described in Appendix 1.

Figure 6*a* shows annual values for the $\theta = 450$ K isentrope. The growth of the ozone hole in the lower stratosphere is primarily influenced by the amount of chemical processing that has taken place within the vortex over the winter (which is enhanced at lower temperatures by greater polar stratospheric cloud volume), and the amount of the vortex that is illuminated by sunlight after the end of the polar night (which depends on the size and symmetry of the vortex). As discussed by Krummel *et al.* (2019), the amount of chemical processing in the vortex for any given year appears to be a stronger influence on the scatter in Fig. 6*a* than the amount of illumination received by the vortex during the formation of the ozone hole. There is a general tendency in Fig. 6*a* for the ozone loss rate to be positively correlated with temperature (Pearson correlation coefficient $r = 0.80$, significant at the 95% confidence limit), with enhanced ozone loss occurring at lower temperatures. On the $\theta = 850$ K isentrope (Fig 6*b*), the correlation between the ozone rate-of-change and temperature is negative ($r = -0.75$, also significant at the 95% confidence limit). At this level, ozone loss is primarily by gas-phase processes which are more efficient at higher temperatures.

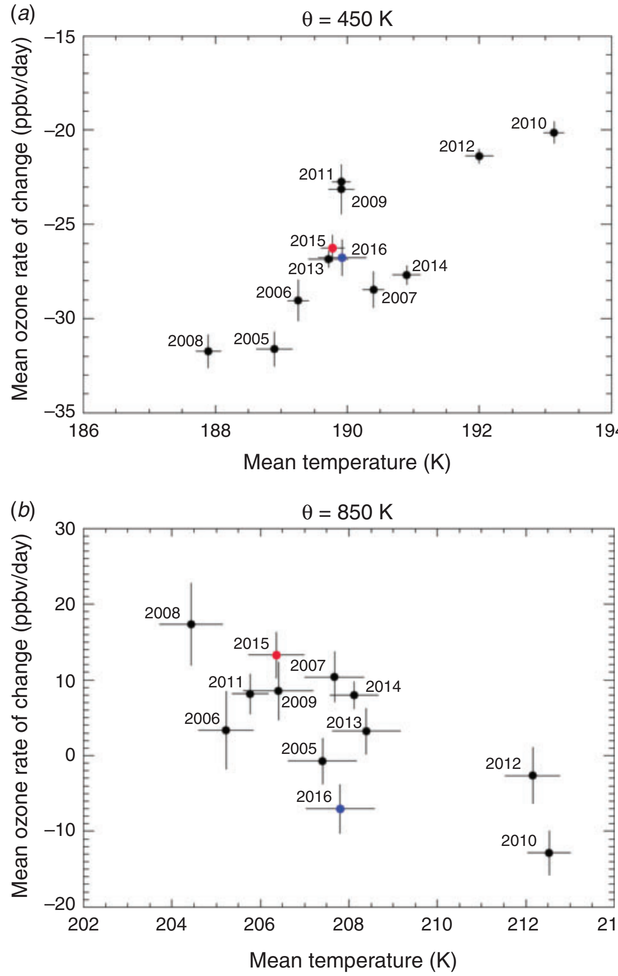

Fig. 6. Vortex-average ozone rate of change vs temperature, averaged between days 200 and 260, on isentropic surfaces of (*a*) $\theta = 450$ K (~18 km altitude) and (*b*) $\theta = 850$ K (~30 km altitude) obtained from MLS v4.2 swath measurements. The vertical and horizontal bars span ± one standard error in the mean of the deseasonalised daily measurements. The base period used to deseasonalise the daily values is 2004–14. The relevant year is indicated immediately adjacent to each value – years 2015 and 2016 are highlighted in red and blue respectively.

Overall, the behaviour of 2015 and 2016 in Fig. 6*a*, *b* appears typical in comparison to years in which the polar vortex during late winter and early spring was relatively undisturbed by dynamical activity. This is consistent with the Davis ozonesonde data (Fig. 4) which show the rate of ozone decline in September was fairly typical in both 2015 and 2016, with only subsequent time periods displaying more distinctive behaviour.

3.3 Ozone measurements at Macquarie Island

The BoM carries out long-term high-quality measurements of total column ozone at Macquarie Island (54.5°S and 158.9°E) using the Dobson spectrophotometer, continuing a program dating back to 1957. Observations for 2015 and 2016 are shown in red in Fig. 7*a*, *b* respectively compared to the 1987–2014 range.

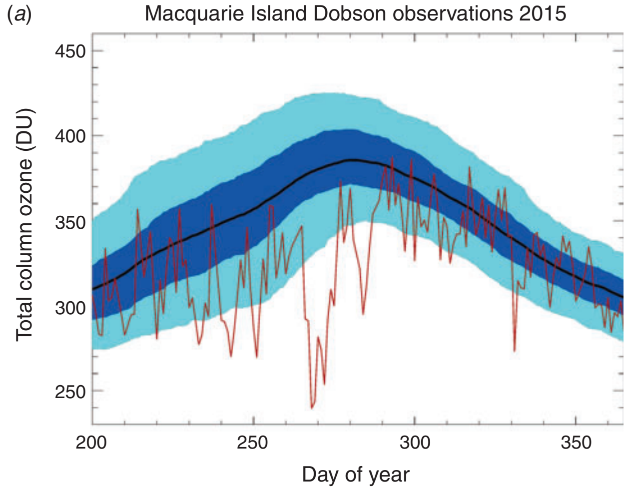

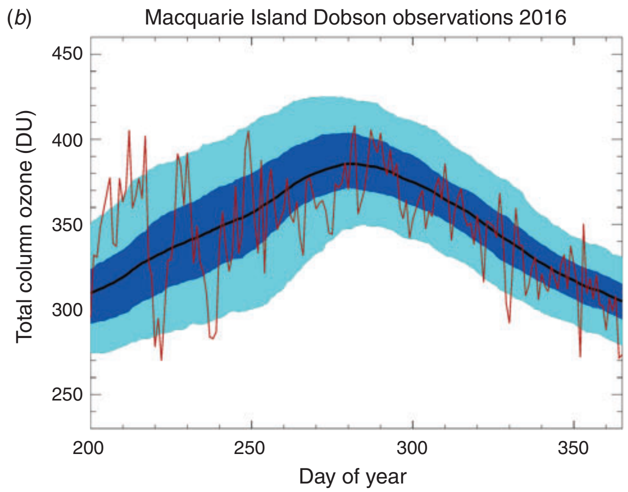

Fig. 7. Daily mean total column ozone observations made by Dobson spectrophotometer at Macquarie Island in (*a*) 2015 and (*b*) 2016 compared to the 1987–2014 range. (The black line shows the smoothed daily median, the dark blue band the 30th–70th percentile range, and the light blue band the 10th–90th percentile range.)

In 2015, total column ozone measurements at Macquarie Island were generally below the long-term mean in winter but returned to more typical values from the middle of October (day 285) onwards. A number of episodes of very low ozone values were observed in September, whereas Macquarie Island was in the vicinity of the polar vortex. On 25 September (day 268), the daily average ozone was 239.5 DU with the lowest single Dobson reading (AD-Direct Sun) of 233 DU. Anomalously low ozone was also recorded during this time as far north as Melbourne (284 DU).

A further episode of low ozone (273 DU) was observed on 27 November (day 331) during the break-up of the ozone hole when Macquarie fell under the influence of the distorted polar vortex.

No episodes of high ozone above the climatological range were observed in 2015.

Compared to 2015, the total ozone measured at Macquarie Island stayed much closer to the long-term seasonal cycle in 2016.

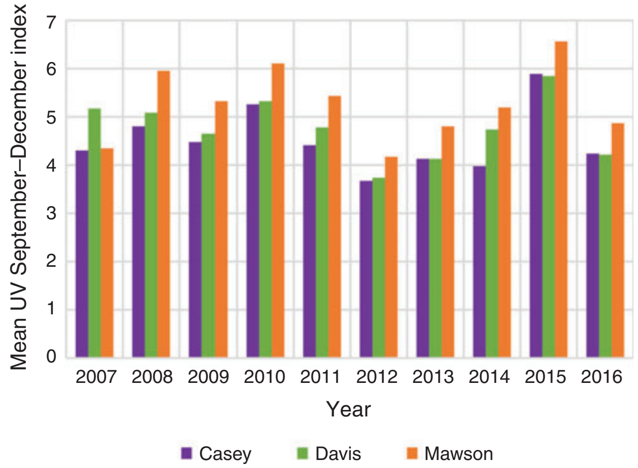

Fig. 8. UV index averaged over September–December for 2007–16 from daily measurements at Casey, Davis and Mawson. At Casey in December 2016, only 5 days of measurements were made.

Two episodes of low ozone were observed though in August when Macquarie Island was influenced by the polar vortex. On 9 August (day 222), a daily average of 269.9 DU was recorded and 282.8 DU on 25 August (day 238). As was the case in 2015, no episodes of high ozone were observed in spring 2016.

3.4 Antarctic ultraviolet radiation

Measurements of biologically effective solar ultraviolet (UV) radiation are made at Casey (66.3°S and 110.5°E), Mawson (67.6°S and 62.9°E) and Davis research stations in Antarctica. Details on the instrumentation and methods used are provided by Tully *et al.* (2008) and Klekociuk *et al.* (2015).

Figure 8 shows the September–December mean UV Index for the three stations from 2007 to 2016. The prolonged low values of total column ozone in October and November (Fig. 1*b*) when the sun is much higher in the sky, resulted in mean UV values being the highest on record at all three stations, exceeding 2010. In 2016, values were significantly lower and broadly consistent with 2013 and 2014. In general, the mean UV values measured each year are strongly rank-correlated with ozone hole breakdown dates as given in column 8 of Table 1, as a longer lasting ozone hole will cause relatively larger UV increases due to the increased solar elevation later in the year.

5 Conclusions

We have examined meteorological conditions and ozone concentrations in the Antarctic atmosphere during 2015 and 2016 using a variety of data sources, including meteorological assimilations, satellite remote sensing measurements, and ground-based instruments and ozonesondes.

The ozone hole of 2015 was one of the most severe on record with respect to maximum area and integrated deficit and was notably long-lasting, with many values above previous extremes in October, November and December. This is attributed to a very strong polar vortex, with the 50 hPa Southern Annular Mode (SAM) at record levels from September to November, and very cold polar temperatures throughout winter and spring – exceeding previous (1979–2014) limits at 100 hPa in October and November. In these conditions, increased concentrations of liquid binary sulfate aerosols resulting from the eruption of the Chilean volcano Calbuco were able to greatly extend the area of the ozone hole equatorward.

In contrast, in 2016, September to November polar temperatures were slightly warmer than the long-term mean in September and October, before warming more markedly in November in conjunction with a weak vortex resulting in an early end to the ozone hole. All assessed metrics for the 2016 ozone hole were at or below their median values.

Acknowledgements

We acknowledge the Department of Environment and Energy for the support of this work, and the assistance of the following people: Jeff Ayton and the AAD's Antarctic Medical Practitioners in collecting the solar UV data, BoM observers for collecting upper air measurements and the expeditioners of the British Antarctic Survey for collecting the Halley measurements. The TOMS, OMI and OMPS data used in this study are provided by the NASA Goddard Space Flight Center, Atmospheric Chemistry & Dynamics Branch, Code 613.3. Aura/MLS data used in this study were acquired as part of the NASA's Earth–Sun System Division and archived and distributed by the Goddard Earth Sciences (GES) Data and Information Services Center (DISC) Distributed Active Archive Center (DAAC). UKMO data were obtained from the British Atmospheric Data Centre (http://badc.nerc.ac.uk, accessed 22 April 2020). NCEP Reanalysis-2 data were obtained from the National Oceanic and Atmospheric Administration Earth System Research laboratory, Physical Sciences Division. Part of this work was performed under Project 4293 of the Australian Antarctic Science programme. This research did not receive any specific grant funding.

References

Baldwin, M. P., and Dunkerton, T. J. (1998). Quasi-biennial modulations of the Southern Hemisphere stratospheric polar vortex. *Geophys. Res. Lett.* **25**, 3343–3346. doi:10.1029/98GL02445

BAS (British Antarctic Survey) (2015). Provisional Monthly Mean Ozone Values for Halley [online]. Available at http://www.antarctica.ac.uk/met/jds/ozone/data/ZOZ5699.DAT [Verified 28 November 2015].

Douglass, A. R., Newman, P. A., and Solomon, S. (2014). The Antarctic ozone hole: an update. *Phys. Today* **67**(7), 42–48. doi:10.1063/PT.3.2449

Fortuin, J. P. F., and Kelder, H. (1998). An ozone climatology based on ozonesonde and satellite measurements. *J. Geophys. Res.* **103**, 31709–31734. doi:10.1029/1998JD200008

Fraser, P., Krummel, P., Steele, P., Trudinger, C., Etheridge, D., Derek, D., O'Doherty, S., Simmonds, P., Miller, B., Muhle, J., Weiss, R., Oram, D., Prinn, R., and Wang R. (2014). Equivalent effective stratospheric chlorine from Cape Grim Air Archive, Antarctic firn and AGAGE global measurements of ozone depleting substances. In 'Baseline Atmospheric Program (Australia) 2009–2010'. (Eds N. Derek, P. Krummel, and S. Cleland.) pp. 17–23. (Australian Bureau of Meteorology and CSIRO Marine and Atmospheric Research: Melbourne, Vic., Australia.)

Ivy, D. J., Solomon, S., Kinnison, D., Mills, M. J., Schmidt, A., and Neely, R. R., III (2017). The influence of the Calbuco eruption on the 2015 Antarctic ozone hole in a fully coupled chemistry-climate model. *Geophys. Res. Lett.* **44**, 2556–2561. doi:10.1002/2016GL071925

Kanamitsu, M., Ebisuzaki, W., Woollen, J., Yang, S.-K., Hnilo, J. J., Fiorino, M., and Potter, G. L. (2002). NCEP-DEO AMIP-II reanalysis (R-2). *Bull. Am. Met. Soc.* **83**(11), 1631–1643. doi:10.1175/BAMS-83-11-1631

Kirner, O., Müller, R., Ruhnke, R., and Fischer, H. (2015). Contribution of liquid, NAT and ice particles to chlorine activation and ozone depletion in Antarctic winter and spring. *Atmos. Chem. Phys.* **15**, 2019–2030. doi:10.5194/ACP-15-2019-2015

Klekociuk, A. R., Tully, M. B., Alexander, S. P., Dargaville, R. J., Deschamps, L. L., Fraser, P. J., Gies, H. P., Henderson, S. I., Javorniczky, J., Krummel, P. B., Petelina, S. V., Shanklin, J. D., Siddaway, J. M., and Stone, K. A. (2011). The Antarctic Ozone hole during 2010. *Aust. Met. Oceanog. J.* **61**, 253–267. doi:10.22499/2.6104.006

Klekociuk, A. R., Tully, M. B., Krummel, P. B., Gies, H. P., Petelina, S. V., Alexander, S. P., Deschamps, L. L., Fraser, P. J., Henderson, S. I., Javorniczky, J., Shanklin, J. D., Siddaway, J. M., and Stone, K. A. (2014*a*). The Antarctic ozone hole during 2011. *Aust. Met. Oceanog. J.* **64**, 293–311. doi:10.22499/2.6404.006

Klekociuk, A. R., Tully, M. B., Krummel, P. B., Gies, H. P., Alexander, S. P., Fraser, P. J., Henderson, S. I., Javorniczky, J., Petelina, S. V., Shanklin, J. D., Schofield, R., and Stone, K. A. (2014*b*). The Antarctic ozone hole during 2012. *Aust. Met. Oceanog. J.* **64**, 313–330. doi:10.22499/2.6404.007

Klekociuk, A. R., Tully, M. B., Krummel, P. B., Gies, H. P., Alexander, S. P., Fraser, P. J., Henderson, S. I., Javorniczky, J., Shanklin, J. D., Schofield, R., and Stone, K. A. (2015). The Antarctic ozone hole during 2013. *Aust. Met. Oceanog. J.* **65**, 247–266. doi:10.22499/2.6502.005

Krummel, P. B., Fraser, P. J. and Derek, N. (2016). The 2015 Antarctic ozone hole and ozone science summary: final report. (Report prepared for the Australian Government Department of the Environment, CSIRO: Australia.) iv, 27 pp. Available at http://www.environment.gov.au/protection/ozone/publications/antarctic-ozone-hole-summary-reports [Verified 21 April 2020].

Krummel, P. B., Fraser P. J. and Derek, N. (2017). The 2016 Antarctic ozone hole summary: final report. (Report prepared for the Australian Government Department of the Environment and Energy, CSIRO: Australia.) v, 28 pp. Available at http://www.environment.gov.au/protection/ozone/publications/antarctic-ozone-hole-summary-reports [Verified 21 April 2020].

Krummel, P. B., Klekociuk, A. R., Tully, M. B., Gies, H. P., Alexander, S. P., Fraser, P. J., Henderson, S. I., Schofield, R., Shanklin, J. D., and Stone, K. A. (2019). The Antarctic. ozone hole during 2014. *J. South. Hemisph. Earth Syst. Sci.* **69**, 1–15. doi:10.1071/ES19023

Langematz, U., Schmidt, F., Kunze, M., Bodeker, G. E., and Braesicke, P. (2016). Antarctic ozone depletion between 1960 and 1980 in observations and chemistry–climate model simulations. *Atmos. Chem. Phys.* **16**, 15619–15627. doi:10.5194/ACP-16-15619-2016

Manney, G. L., Daffer, W. H., Zawodny, J. M., Bernath, P. F., Hoppel, K. W., Walker, K. A., Knosp, B. W., Boone, C., Remsberg, E. E., Santee, M. L., Harvey, V. L., Pawson, S., Jackson, D. R., Deaver, L., McElroy, C. T., McLinden, C. A., Drummond, J. R., Pumphrey, H. C., Lambert, A., Schwartz, M. J., Froidevaux, L., McLeod, S., Takacs, L. L., Suarez, M. J., Trepte, C. R., Cuddy, D. C., Livesey, N. J., Harwood, R. S., and Waters (2007). Solar occultation satellite data and derived meteorological products: Sampling issues and comparisons with Aura Microwave Limb Sounder. *J. Geophys. Res.* **112**, D24S50. doi:10.1029/2007JD008709

Marshall, G. J. (2003). Trends in the Southern Annular Mode from observations and reanalyses. *J. Clim.* **16**, 4134–4143. doi:10.1175/1520-0442(2003)016<4134:TITSAM>2.0.CO;2

Nash, E. R., Newman, P. A., Rosenfield, J. E., and Schoeberl, M. R. (1996). An objective determination of the polar vortex using Ertel's potential vorticity. *J. Geophys. Res.* **101**(D5), 9471–9478. doi:10.1029/96JD00066

Schwartz, M. J., Lambert, A., Manney, G. L., Read, W. G., Livesey, N. J., Froidevaux, L., Ao, C. O., Bernath, P. F., Boone, C. D., Cofield, R. E., Daffer, W. H., Drouin, B. J., Fetzer, E. J., Fuller, R. A., Jarnot, R. F., Jiang,

J. H., Jiang, Y. B., Knosp, B. W., Krüger, K. R., Li, J.-L. F., Mlynczak, M. G., Pawson, S., Russell, J. M., III, Santee, M. L., Snyder, W. V., Stek, P. C., Thurstans, R. P., Tompkins, A. M., Wagner, P. A., Walker, K. A., Waters, J. W., and Wu, D. L. (2008). Validation of the Aura Microwave Limb Sounder temperature and geopotential height measurements. *J. Geophys. Res.* **113**, D15S11. doi:10.1029/2007JD008783

Solomon, S., Haskins, J., Ivy, D. J., and Min, F. (2014). Fundamental differences between Arctic and Antarctic ozone depletion. *Proc. Natl. Acad. Sci. USA* **111**(17), 6220–6225. doi:10.1073/PNAS.1319307111

Solomon, S., Kinnison, D., Bandoro, J., and Garcia, R. (2015). Simulation of polar ozone depletion: an update. *J. Geophys. Res. Atmos* **120**, 7958–7974. doi:10.1002/2015JD023365

Solomon, S., Ivy, D. J., Kinnison, D., Mills, M. J., Neely, R. R., III, and Schmidt, A. (2016). Emergence of healing in the Antarctic ozone layer. *Science* **252**(6296), 269–274. doi:10.1126/SCIENCE.AAE0061

Stone, K. A., Solomon, S., Kinnison, D. E., Pitts, M. C., Poole, L. R., Mills, M. J., Schmidt, A., Neely, R. R., III, Ivy, D., Schwartz, M. J., Vernier, J.-P., Johnson, B. J., Tully, M. B., Klekociuk, A. R., König-Langlo, G., and Hagiya, S. (2017). Observing. the impact of Calbuco volcanic aerosols on South Polar ozone depletion in 2015. *J. Geophys. Res.* **122**, 11862–11879. doi:10.1002/2017JD026987

Strahan, S. E., Douglass, A. R., Newman, P. A., and Steenrod, S. D. (2014). Inorganic chlorine variability in the Antarctic vortex and implications for ozone recovery. *J. Geophys. Res. Atmos.* **119**, 14098–14109. doi:10.1002/2014JD022295

Strahan, S. E., Oman, L. D., Douglass, A. R., and Coy, L. (2015). Modulation of Antarctic vortex composition by the quasi-biennial oscillation. *Geophys. Res. Lett.* **42**, 4216–4223. doi:10.1002/2015GL063759

Swinbank, R., and O'Neill, A. A. (1994). Stratosphere-troposphere data assimilation system. *Mon. Wea. Rev.* **122**, 686–702. doi:10.1175/1520-0493(1994)122<0686:ASTDAS>2.0.CO;2

Tully, M. B., Klekociuk, A. R., Deschamps, L. L., Henderson, S. I., Krummel, P. B., Fraser, P. J., Shanklin, J. D., Downey, A. H., Gies, H. P., and Javorniczky, J. (2008). The 2007 Antarctic ozone hole. *Aust. Met. Mag.* **57**, 279–298.

Tully, M. B., Klekociuk, A. R., Alexander, S. P., Dargaville, R. J., Deschamps, L. L., Fraser, P. J., Gies, H. P., Henderson, S. I., Javorniczky, J., Krummel, P. B., Petelina, S. V., Shanklin, J. D., Siddaway, J. M., and Stone, K. A. (2011). The Antarctic ozone hole during 2008 and 2009. *Aust. Met. Oceanog. J.* **61**, 77–90. doi:10.22499/2.6101.007

Watson, P. A. G., and Gray, L. G. (2014). How does the Quasi-Biennial Oscillation affect the stratospheric polar vortex. *J. Atmos. Sci.* **71**, 391–409. doi:10.1175/JAS-D-13-096.1

Weber, M., Steinbrecht, W., Roth, C., Coldewey-Egbers, M., Degenstein, D., Fioletov, Y. E., Frith, S. M., Froidevaux, L., de Laat, J., Long, C. S., Loyola, D., and Wild, J. D. (2016). Stratospheric Ozone [in "State of the Climate in 2015"]. *Bull. Am. Meteor. Soc.* **97**(8), S49–S51.

Weber, M., Steinbrecht, W., Frith, S. M., Tweedy, O., Coldewey-Egbers, M., Davis, S., Degenstein, D., Fioletov, Y. E., Froidevaux, L., de Laat, J., Long, C. S., Loyola, D., Roth, C., and Wild, J. D. (2017). Stratospheric ozone [in "State of the Climate in 2016"]. *Bull. Am. Meteor. Soc.* **98**, S49–S51. doi:10.1175 /2017BAMSSTATEOFTHECLIMATE.1

Zhu, Y., Toon, O. B., Pitts, M. C., Lambert, A., Bardeen, C., and Kinnison, D. E. (2017). Comparing simulated PSC optical properties with CALIPSO observations during the 2010 Antarctic winter. *J. Geophys. Res. Atmos.* **122**, 1175–1202. doi:10.1002/2016JD025191

Appendix 1. Supplementary information

A1.1 Polar temperatures and atmospheric indices

Figure A1.1*a* shows monthly mean temperature anomalies for the latitude range 90–65°S from the National Centers for

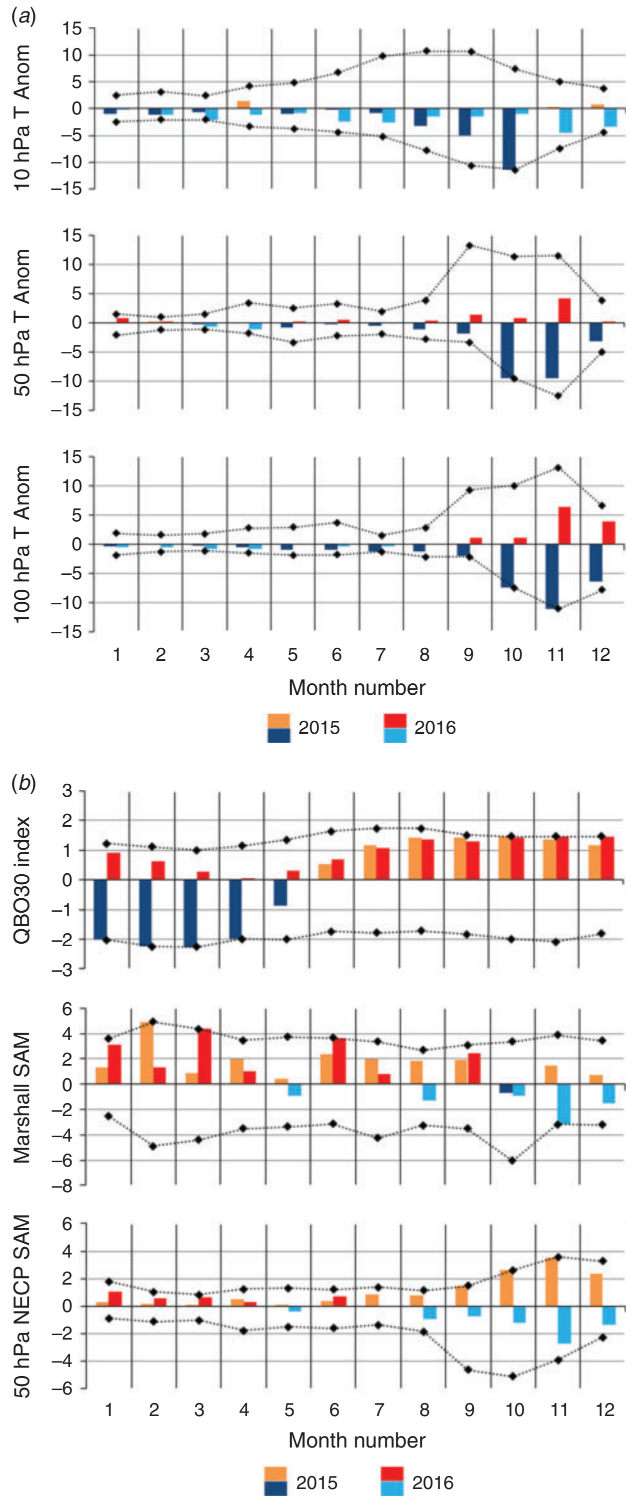

Fig. A1.1. (continued)

Fig. A1.1. (*a*) Monthly temperature anomalies (K) from zonal means for the latitude range 65–90°S from NCEP Reanalysis-2 data relative to the monthly climatology for 1979–2014 at pressure levels of 10 hPa (top), 50 hPa (middle) and 100 hPa (bottom). Coloured bars show monthly anomalies for 2015 and 2016 (legend at bottom), and diamonds connected by solid lines show maximum and minimum anomalies for 1979–2016. (*b*) Monthly (top) NCEP standardised 30 hPa QBO index, (middle) standardised surface SAM index (Marshall 2003) and (bottom) standardised SAM index evaluated at 50 hPa (see text for details). Coloured bars show monthly anomalies for 2015 and 2016 (legend at bottom). The indices are expressed in standard deviations relative to base period of 1981–2010 (for QBO) and 1979–2000 (for SAM). Diamonds connected by solid lines show maximum and minimum anomalies for each index over the period 1979–2016.

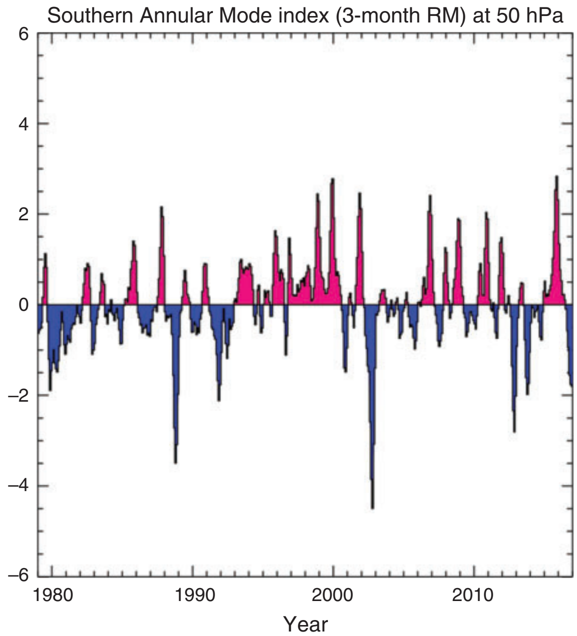

Fig. A1.2. Smoothed monthly Southern Annular Mode index (smoothed with a 3-month running mean) for 1979–2016 for 50 hPa derived from Empirical Orthogonal Function analysis of NCEP Reanalysis-2 geopotential height anomalies poleward of 20°S. The index is expressed in standard deviations relative to the base period 1979–2000. The methodology is described at http://www.cpc.ncep.noaa.gov/products/precip/CWlink/daily_ao_index/history/method.shtml, accessed 21 April 2020.

Environmental Prediction (NCEP) Reanalysis-2 data (Kanamitsu *et al.* 2002) with respect to the base period 1979–2014 for three pressure levels. Temperatures in winter were only slightly below the long-term base period mean but become more anomalously cold in September and particularly October, continuing on into November in the lower levels (50 and 100 hPa). In 2016, the 50 and 100 hPa temperatures were only slightly above the long-term mean but were more markedly warmer in November. The 10 hPa temperatures remained slightly below the mean throughout 2016.

The NCEP standardised 30 hPa quasi-biennial oscillation (QBO) index (http://www.cpc.ncep.noaa.gov/data/indices/qbo.u30.index, accessed 21 April 2020) is shown in the top panel of Fig. A1.1*b*. The QBO modulates the ability of upward

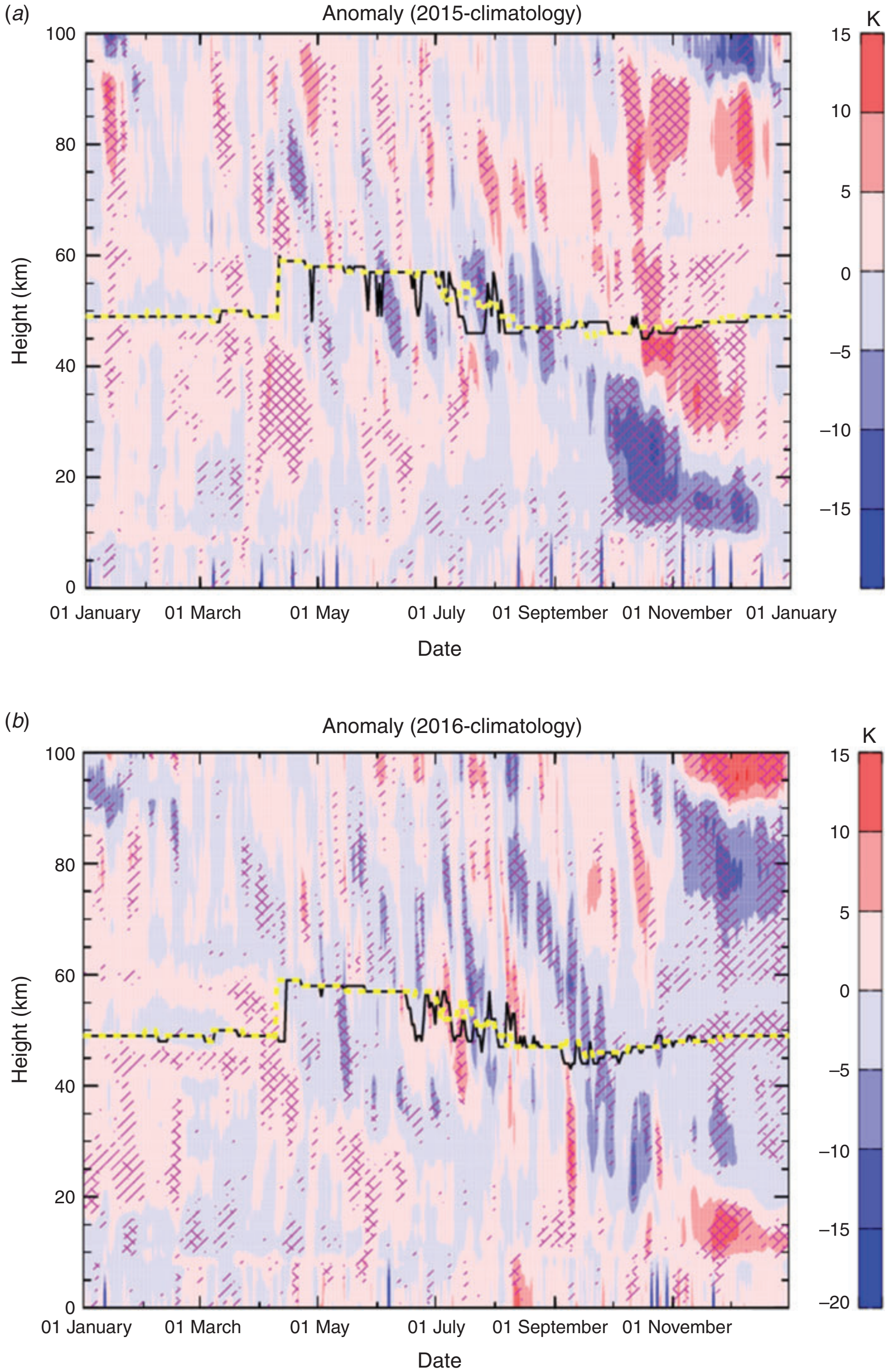

Fig. A1.3. Daily time-height section of anomalies of the zonal average air temperature over latitudes 65–85°S from Aura MLS quality-controlled version 4.2 data for (*a*) 2015 and (*b*) 2016. The anomalies are evaluated relative to the base period of 8 August 2004 (the start of measurements) to 31 December 2014. The solid black line marks the height of the warm-point stratopause for the particular year, whereas the yellow dashed line marks the average warm-point stratopause height over the climatological period. Single diagonal hatches marks anomalies that are outside the interdecile range over the climatological period. Crossed diagonal hatching marks anomalies that exceed the daily maximum or minimum value during the climatological period.

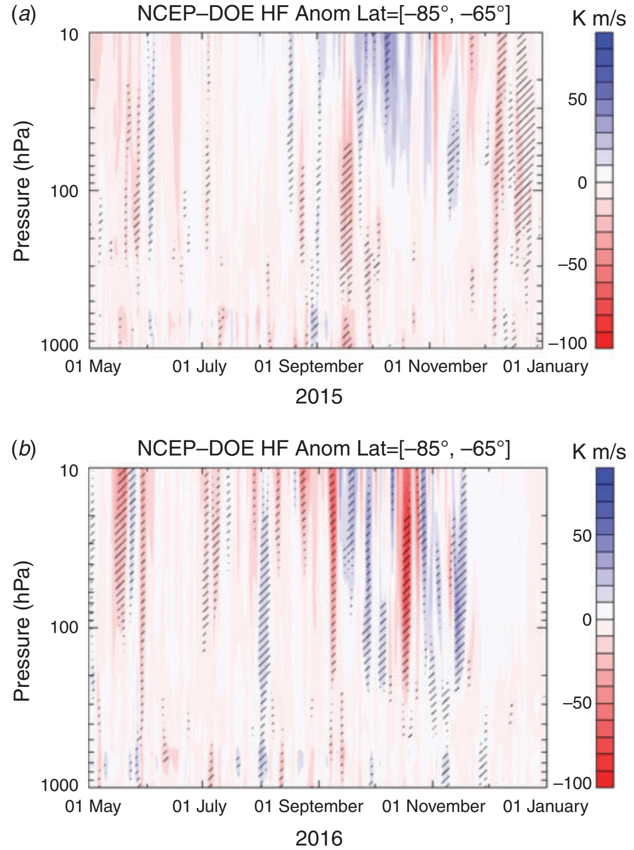

Fig. A1.4. Daily eddy heat flux averaged between the latitudes of 85–65°S as a function of pressure between May and December for (*a*) 2015 and (*b*) 2016 evaluated from UKMO stratospheric assimilated data (Swinbank and O'Neill 1994). Negative values indicate poleward transport of heat. The zero contour is outlined in white.

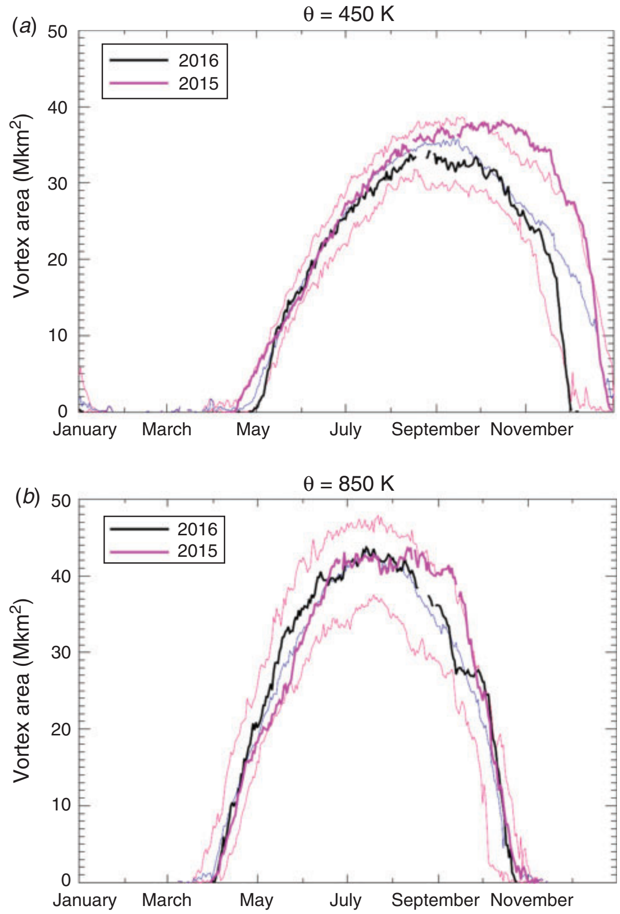

Fig. A1.5. Southern Hemisphere vortex area evaluated on isentropic surfaces of (*a*) $\theta = 450$ K (~18 km height) and (*b*) $\theta = 850$ K (~31 km height). The time-series for 2015 is shown in magenta; 2016 is shown in black the blue time-series is the mean for 1992–2014, whereas the lower and upper red time-series in each graph show the 5th and 95th percentiles respectively for 1992–2014. The vortex area is evaluated using data from the UKMO stratospheric assimilation and represents the surface area enclosed by potential vorticity contours of (*a*) −30 PVU and (*b*) −600 PVU.

propagating planetary waves to influence extratropical latitudes in the winter hemisphere, and the strongly negative phase observed in the first 4 months of 2015, favoured a stronger and less disturbed polar vortex (Baldwin and Dunkerton 1998; Watson and Gray 2014). The phase of the QBO shifted to positive in June 2015 but then, in an unprecedented disruption, remained positive in mid-2016 rather than transitioning to negative.

The middle and lower panels of Fig. A1.1*b* show version of the Southern Annular Mode (SAM) index, defined respectively for the surface (Marshall 2003; http://www.antarctica.ac.uk/met/gjma/sam.html, accessed 21 April 2020) and the stratosphere 50 hPa values evaluated using empirical orthogonal function analysis of NCEP Reanalysis-2 data, following the approach used by the NOAA Climate Prediction Center for their 700 hPa Antarctic Oscillation index (http://www.cpc.ncep.noaa.gov/products/precip/CWlink/daily_ao_index/aao/aao_index.html, accessed 21 April 2020). See Klekociuk *et al.* (2015) for a discussion of the significance of SAM index values in relation to tropospheric and stratospheric wave dynamics.

In line with the polar temperature, the 50 hPa SAM was at the highest level recorded in September, October and November 2015 but was below the long-term mean in spring 2016, particularly in November. The extreme strength of the stratospheric SAM in 2016 is further emphasised in Fig. A1.2 in which the value of the 3-month running mean for 50 hPa was the highest on record.

Daily temperature anomalies averaged over the Antarctic region obtained from measurements by the MLS on the Aura spacecraft (Schwartz *et al.* 2008) are shown for 2015 and 2016 in Fig. A1.3. In 2015, the extreme cold temperatures in October persisted into November and December in the lower stratosphere, but the upper stratosphere was warm from mid-November onwards.

A1.2 Dynamical activity

The poleward transport of heat provides a useful indicator of dynamical disturbances to the polar atmosphere produced by planetary waves at low and mid-latitudes. Fig. A1.4 shows the

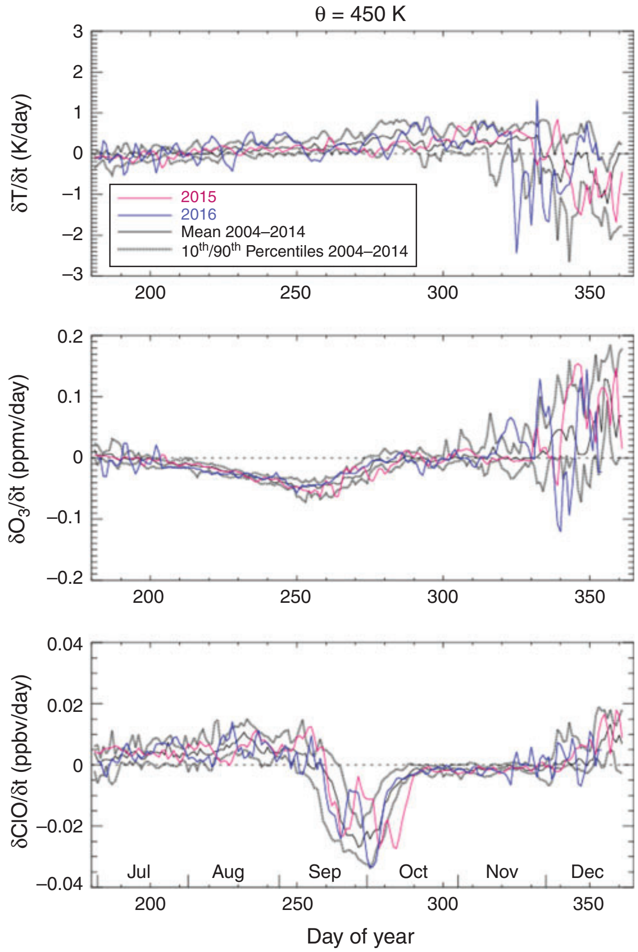

Fig. A1.6. Time derivative time-series of vortex-average parameters on $\theta = 450\,\mathrm{K}$ isentropic surface obtained from Aura MLS v4.2 daily swath measurements. Top: temperature (T) time derivative. Middle: ozone (O_3) mixing ratio time derivative. Bottom: chlorine monoxide (ClO) mixing ratio time derivative. Daily values are shown for 2015 (red line), 2016 (blue line), the mean for 2004–16 black line), and the 10th and 90th percentiles over 2004–14 (dashed grey line). To produce the daily data, swath profiles passing the recommended MLS data quality criteria were interpolated to each isentropic surface and then averaged within the inner edge of the polar vortex defined by Nash *et al.* (1996) using information provided by the MLS derived meteorological product (Manney *et al.* 2007) version GEOS5-MERRA2. A 7-day running average (windowed ± 3 days and requiring at least 4 days to be present in each average) was then applied to the daily values before calculating the time derivative. Because the first MLS measurements were made on 8 August 2004, and subsequent measurements are not available for all days, daily averages and percentiles are not necessarily evaluated over all years between 2004 and 2014.

evolution of heat flux (measured by the product of the zonal anomalies in temperature and meridional wind speed) in the polar cap region during 2015 and 2016 using assimilated meteorological data from the United Kingdom Meteorological Office (UKMO).

In 2015, the heat flux was at or below mean levels between 10 and 100 hPa for most of the period of July to November, the accumulated result of which led to a markedly undisturbed vortex. One modest warming event is evident in mid-September in the lower stratosphere.

In 2016, two pronounced warming events were evident in early September and again in late October, the latter of which resulted in a decrease in the ozone hole area and warm temperatures from that time on. Wave activity was distinctly below the long-term mean for a brief period around the beginning of October.

A1.3 The polar vortex

Time-series of proxies for the areal extent of the stratospheric polar vortex are shown in Fig. A1.5 for the $\theta = 450\,\mathrm{K}$ and $\theta = 850\,\mathrm{K}$ isentropic surfaces. At the $\theta = 450\,\mathrm{K}$ level the size of the 2015 vortex departed markedly from the long-term mean in late September and exceeded the previous maximum in October and November. The 2016 vortex at the same level was of typical size in winter but was somewhat smaller in September and dissipated abruptly at the end of November. The size of the vortex at $\theta = 850\,\mathrm{K}$ in both years was mostly close to the long-term mean, except for a period in September and early October when the size was close to the maximum of the base period. As seen in Fig. A1.3, the cold conditions in 2015 only persisted in October and November in the lower stratosphere.

Daily time-series of vortex-average time-derivatives of temperature, ozone mixing ratio and chlorine monoxide (ClO) mixing ratio for isentropic levels of $\theta = 450\,\mathrm{K}$ ($\sim$18 km height) and $\theta = 850\,\mathrm{K}$ ($\sim$31 km height) are shown for 2015 in Fig. A1.6*a*, *b* respectively along with climatological means and percentiles. The time-series are constructed using soundings from the Aura MLS, and estimates of the vortex edge location are derived from the MERRA-2 meteorological reanalysis (Manney *et al.* 2007). As discussed by Manney *et al.* (2007), location of the vortex edge can be problematic, particularly outside of winter in the lower stratosphere, and no account has been made here for biases introduced by incorrect diagnosis of the vortex position.